# Methods in Computational Neuroscience: Firing rate models and dynamical systems

Sepehr SAEEDPOUR

April 29, 2025

## Introduction

This is a brief introduction about the assignment topic.

## 1 Neuron with self-connection

### 1.1 Plot the activation function

The activation function $f(s) = 60(1 + \tanh(s))$ maps the total input to the neuron's firing rate. This sigmoidal function has several key properties: output range of $[0, 120]$ spikes per second, centered at $f(0) = 60$ spikes per second, and asymptotic behavior approaching 0 for very negative inputs and 120 for very positive inputs.

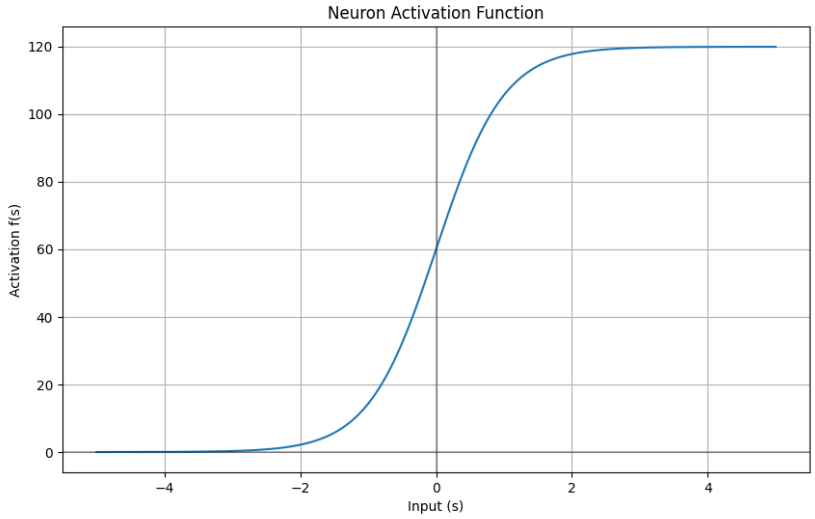


Figure 1: Plot of the activation function $f(s) = 60(1 + \tanh(s))$ over the input range $[-5, 5]$. The function shows the characteristic S-shape of a sigmoid, with output values ranging from 0 to 120 spikes per second.

### 1.2 Study the dynamics

When simulating the system with three initial conditions $r(0) = 59$, $r(0) = 60$, and $r(0) = 61$, I observe interesting dynamical behavior:

- For $r(0) = 59$: The firing rate decreases and settles at the lower stable fixed point.
- For $r(0) = 60$: The firing rate remains constant, indicating this is an unstable fixed point.
- For $r(0) = 61$: The firing rate increases and settles at the higher stable fixed point.

This behavior indicates the system has three fixed points, with the middle one ($r \approx 60$) acting as a threshold. Initial conditions below this threshold lead to a low firing rate state, while initial conditions above it lead to a high firing rate state. This is characteristic of a bistable system.

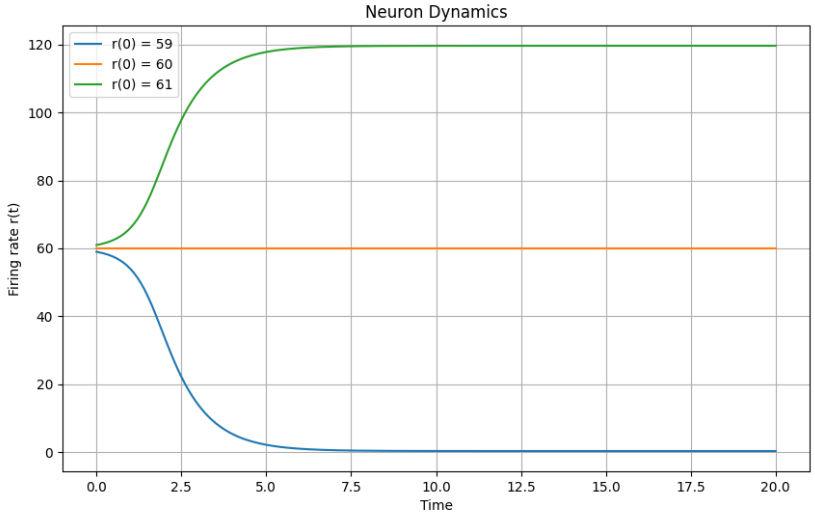


Figure 2: Time evolution of the neuron firing rate $r(t)$ with three different initial conditions: $r(0) = 59$, $r(0) = 60$, and $r(0) = 61$. The trajectories demonstrate the bistable nature of the system, with two stable fixed points separated by an unstable threshold at $r \approx 60$.

### 1.3 Add noise - NOT FINAL

Adding noise to the system reveals additional insights:

$$\frac{dr(t)}{dt} = -r(t) + f(wr(t) + I) + \sigma\eta(t) \tag{1}$$

Where $\eta(t)$ is Gaussian white noise and $\sigma$ is the noise magnitude.

- **(a) Low noise** ($\sigma = 0.1$): The system mostly maintains its bistable behavior, exhibiting only small stochastic excursions around the two attracting fixed points. A trajectory that starts near $r_0 \approx 60\,\text{Hz}$ drifts away because this intermediate firing rate is an *unstable* fixed point, so the rate does *not* remain constant there.
- **(b) Medium noise** ($\sigma = 1.0$): Larger fluctuations occasionally push trajectories across the separatrix, so the neuron sometimes switches between low- and high-firing states.
- **(c) High noise** ($\sigma = 5.0$): Noise dominates the dynamics; trajectories hop back and forth between the two attractors so frequently that the system effectively loses any memory of its initial condition.

This demonstrates how noise can induce transitions between stable states in a bistable system, with the frequency of transitions increasing with noise magnitude.

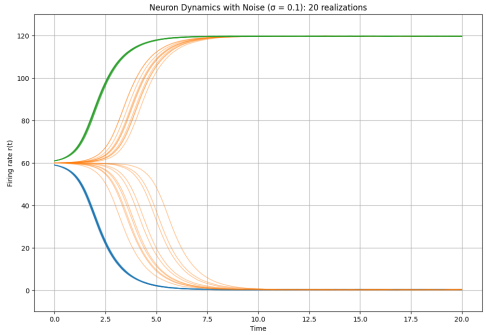


(a) Low noise ($\sigma = 0.1$)

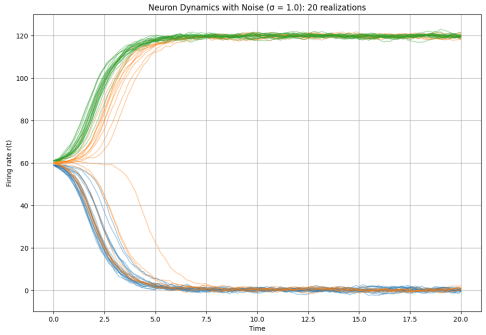


(b) Medium noise ($\sigma = 1.0$)

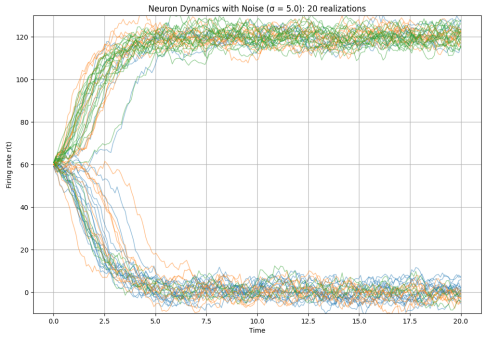


(c) High noise ($\sigma = 5.0$)

Figure 3: Effect of different noise levels on the neuron dynamics. As noise magnitude increases, transitions between stable states become more frequent, demonstrating how noise can induce state switching in a bistable system.

## 1.4 Study the flux

The flux analysis examines the derivative $\frac{dr}{dt}$ as a function of the firing rate $r$. The plot of this flux function reveals:

- Three zero-crossings (fixed points) where $\frac{dr}{dt} = 0$:
  1. Lower fixed point: Stable (negative slope at crossing)
  2. Middle fixed point: Unstable (positive slope at crossing)
  3. Upper fixed point: Stable (negative slope at crossing)

The stability of these fixed points can be determined by the slope of the flux function at each crossing:

- Negative slope: Stable fixed point (perturbing the system slightly causes it to return to the fixed point)
- Positive slope: Unstable fixed point (perturbing the system slightly causes it to move away from the fixed point)

These findings confirm our observations from the time series simulations, providing a deeper understanding of the bistable nature of the system.

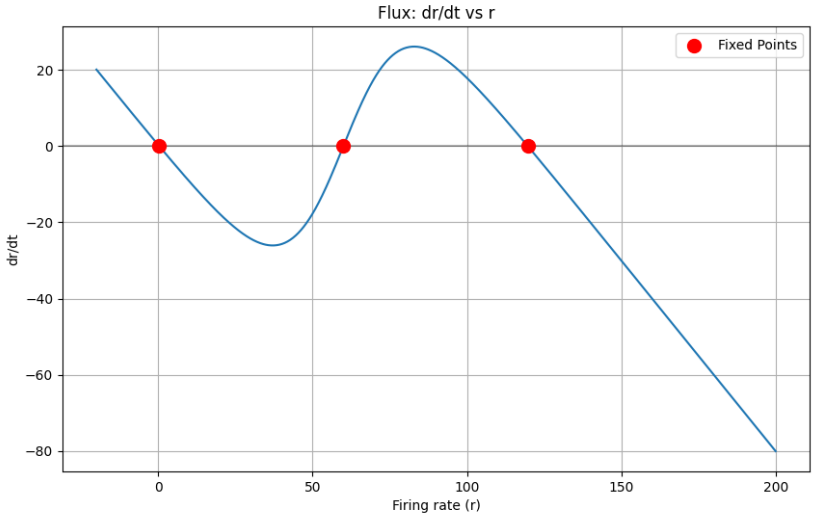


Figure 4: Flux analysis showing $\frac{dr}{dt}$ as a function of firing rate $r$. The zero-crossings represent fixed points of the system. The middle fixed point has a positive slope (unstable), while the other two have negative slopes (stable), confirming the bistable nature of the system.

## 1.5 Bifurcation diagram

The bifurcation diagram explores how the number and nature of fixed points change as system parameters (synaptic strength $w$ and external input $I$) vary. The analysis reveals:

- For low values of $w$ (weak self-connection): The system has a single stable fixed point.
- For higher values of $w$: The system exhibits bistability with three fixed points (two stable, one unstable).

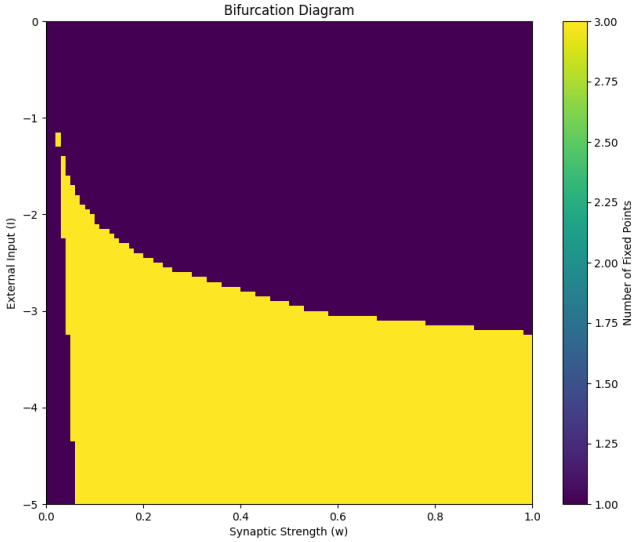


Figure 5: Bifurcation diagram showing how the number of fixed points changes with synaptic strength ($w$) and external input ($I$). Different colors represent different numbers of fixed points. The boundaries between regions represent bifurcation points where the qualitative behavior of the system changes.

# 2 2D network: mutual excitation

## 2.1 Plot the dynamics

The time evolution of the firing rates $x(t)$ and $y(t)$ was simulated for different initial conditions. The differential equations were integrated numerically using the Euler method with a time step of $dt = 0.1$.

Figure 6 shows the evolution of the firing rates over time for four different initial conditions.

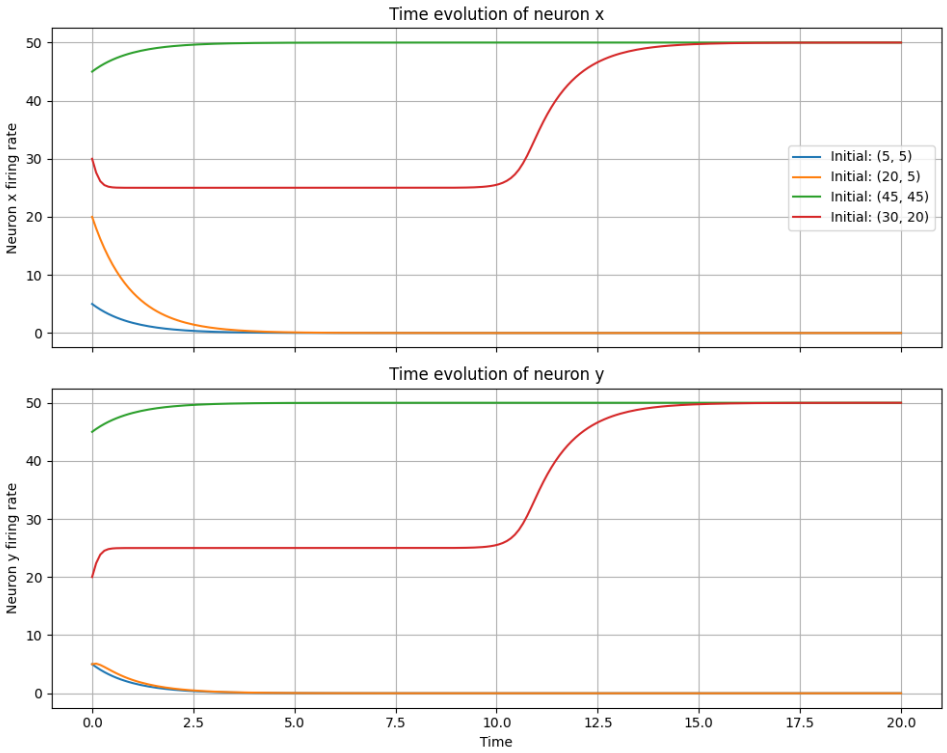


Figure 6: Time evolution of the firing rates $x(t)$ and $y(t)$ for different initial conditions. The top panel shows the firing rate of neuron $x$, and the bottom panel shows the firing rate of neuron $y$.

From the time evolution plots, we can observe that:

- Initial conditions starting near $[5, 5]$ converge to zero firing rates (both neurons shut down).
- Initial conditions starting near $[45, 45]$ converge to a high firing rate fixed point.
- The middle-low and mixed initial states show interesting transient dynamics before eventually converging to either zero firing rate or a high firing rate fixed point.

This suggests that the system exhibits bistability, with two stable fixed points (attractors) and a saddle point that separates their basins of attraction.

## 2.2 State space

The trajectories in state space (plotting $x$ versus $y$) provide a more comprehensive view of the dynamics. Figure 7 shows these trajectories for seven different initial conditions.

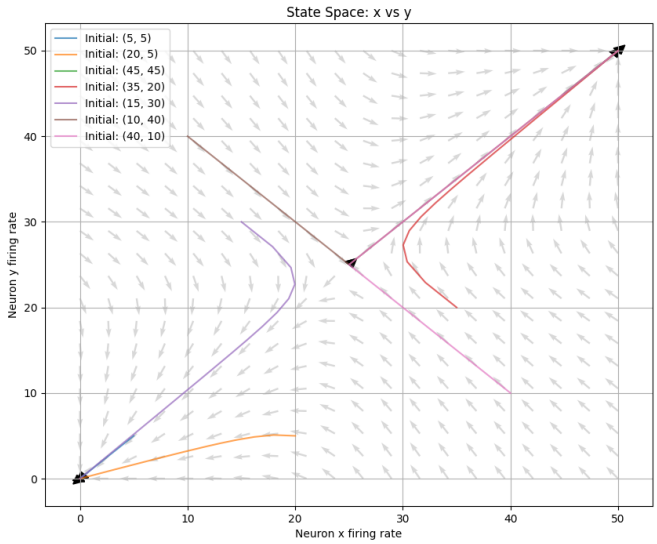


Figure 7: State space trajectories for different initial conditions. Arrows indicate the direction of movement along each trajectory. They show that trajectories starting on one side of the saddle's stable manifold flow to the low-rate rest state, while those on the other side are driven to the high-rate self-excited state, revealing bistability.

## 2.3 Nullclines

Nullclines are curves in the state space where the derivative of one variable is zero. For this system:

- $x$-nullcline: $\frac{dx}{dt} = 0 \implies x = f(w_2 y + I) = f(0.4y - 10)$
- $y$-nullcline: $\frac{dy}{dt} = 0 \implies y = f(w_1 x + I) = f(0.4x - 10)$

Figure 8 shows the nullclines plotted in the state space.

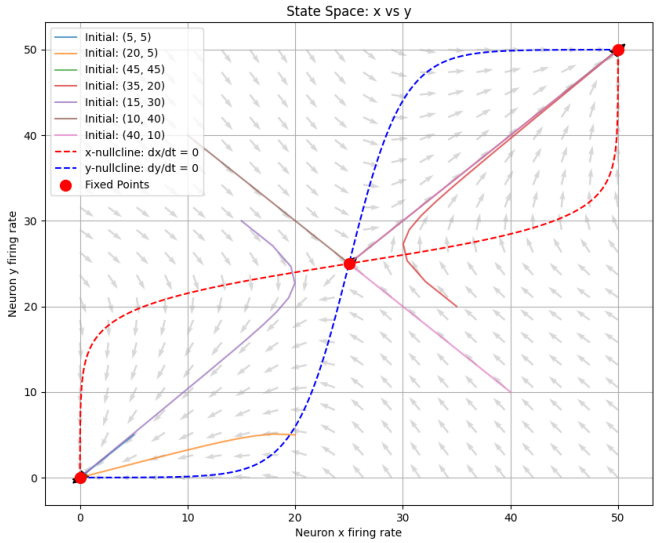


Figure 8: Nullclines of the system. The red dashed line represents the $x$-nullcline ($dx/dt = 0$), the blue dashed line represents the $y$-nullcline ($dy/dt = 0$), and red dots represent fixed points.

Along the red $x$-nullcline ($\dot{x} = 0$) the horizontal flow changes sign— arrows point left ($\dot{x} < 0$) to its left and right ($\dot{x} > 0$) to its right— while along the blue $y$-nullcline ($\dot{y} = 0$) the vertical flow is upward ($\dot{y} > 0$) below and downward ($\dot{y} < 0$) above. Because the sigmoid is S-shaped, the nullclines bend sharply around the threshold 0.4(x or y) − 10 = 25.

## 2.4 Fixed points

The fixed points of the system are located at the intersections of the nullclines (Figure 8). Solving the system numerically:

$$\begin{cases} x = f(0.4y - 10) \\ y = f(0.4x - 10) \end{cases} \tag{2}$$

We find three fixed points:

1. Low firing rate fixed point: approximately at $[x, y] \approx [0, 0]$
2. Middle firing rate fixed point: approximately at $[x, y] \approx [25, 25]$
3. High firing rate fixed point: approximately at $[x, y] \approx [50, 50]$

- **Stable attractors.** Trajectories drift toward the low-rate node near zero and toward the high-rate node close to saturation, demonstrating that both equilibria are stable.
- **Unstable saddle.** At moderate activity the trajectories reach a fixed point that is stable along one manifold (y = -x) and unstable along the orthogonal one (y = x). This exactly aligns with the signature of a saddle.

The state-space therefore contains two attracting fixed points—one at low ($x = y \approx 0$) and one at high ($x = y \approx 50$) firing rates separated by an unstable saddle at $x = y = 25$. State-space trajectories illustrate how every initial condition eventually settles into one of the two attractors, with the saddle acting as a boundary between them.

## 2.5 Study the stability of the fixed points analitically

To analyze the stability of the fixed points analytically, we compute the Jacobian matrix of the system:

$$J = \begin{bmatrix} \frac{\partial}{\partial x}\left(-x + f(w_2 y + I)\right) & \frac{\partial}{\partial y}\left(-x + f(w_2 y + I)\right) \\ \frac{\partial}{\partial x}\left(-y + f(w_1 x + I)\right) & \frac{\partial}{\partial y}\left(-y + f(w_1 x + I)\right) \end{bmatrix} = \begin{bmatrix} -1 & w_2 f'(w_2 y + I) \\ w_1 f'(w_1 x + I) & -1 \end{bmatrix} \tag{3}$$

where $f'(s) = \frac{df}{ds} = 50\sigma(s)(1 - \sigma(s))$, the derivative of our activation function.
For each fixed point $(x^*, y^*)$, we evaluate the Jacobian and determine its eigenvalues:

$$\lambda_{1,2} = \frac{\text{tr}(J)}{2} \pm \sqrt{\frac{(\text{tr}(J))^2}{4} - \det(J)}$$

The stability of each fixed point is determined by the eigenvalues:

- If all eigenvalues have negative real parts, the fixed point is stable (attractor)
- If any eigenvalue has a positive real part, the fixed point is unstable
- If eigenvalues have opposite signs, the fixed point is a saddle point

Fixed point classification based on the determinant and trace:

- $\det(J) < 0$: Saddle point (unstable)
- $\det(J) > 0, \text{tr}(J) < 0$: Stable node or spiral
- $\det(J) > 0, \text{tr}(J) > 0$: Unstable node or spiral

At the low fixed point $(x^*, y^*) \approx (0, 0)$, the derivatives $f'$ are nearly zero because inputs are far below threshold, making $\det(J) \approx 1$ and $\text{tr}(J) \approx -2$, yielding eigenvalues $\lambda_{1,2} \approx -1$. This confirms it's a stable node.

At the middle fixed point $(x^*, y^*) \approx (25, 25)$, the derivatives $f'$ are near maximum, and with $w_1 = w_2 = 0.4$, we get $\det(J) = -24 < 0$, confirming it's a saddle point with one positive (4) and one negative (-6) eigenvalue.

At the high fixed point $(x^*, y^*) \approx (50, 50)$, similar to the low fixed point, the derivatives are small as inputs are far above threshold, giving $\det(J) > 0$ and $\text{tr}(J) < 0$, confirming it's a stable node.

| **Fixed Point** | **Eigenvalues** | **Determinant** | **Classification** |
|---|---|---|---|
| Low $(0, 0)$ | Both negative | Positive | Stable node |
| Middle $(25, 25)$ | One positive, one negative | Negative | Saddle point |
| High $(50, 50)$ | Both negative | Positive | Stable node |

Table 1: Stability analysis results for the three fixed points. The bistable behavior arises from having two stable nodes separated by a saddle point.

This analytical stability analysis confirms our observations from the state space trajectories and explains the system's bistable behavior, with the saddle point forming the boundary between the basins of attraction of the two stable states.

## 2.6 Bifurcation diagram

The bifurcation diagram shows how the number and position of fixed points change as the external input current $I$ varies from $-20$ to $-10$.

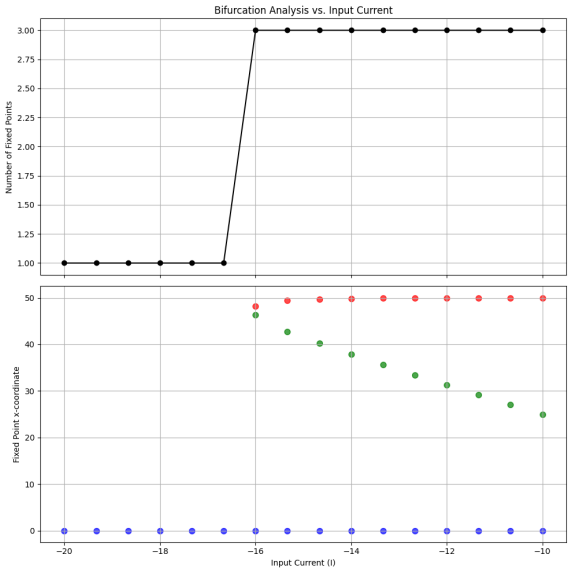


(a) Bifurcation diagram showing the number of fixed points (top) and the $x$-coordinates of fixed points (bottom) as a function of external input $I$.

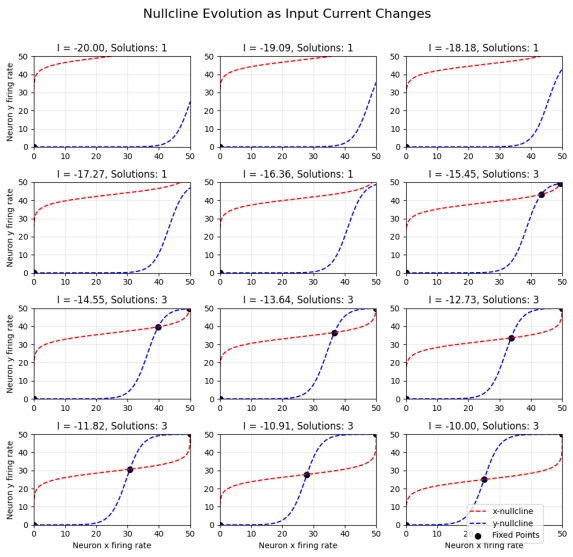


(b) Evolution of nullclines as $I$ changes. The intersections of nullclines are fixed points of the system, showing how they emerge with changing input.

Figure 9: Analysis of system dynamics as a function of external input current $I$.

From the bifurcation diagram, we observe how the fixed point structure changes with input current $I$. The bifurcation point occurs at approximately $I \approx -16$ where saddle-node bifurcation takes place.

From the bifurcation diagram, we can identify distinct regimes:

- For very negative input ($I < -16$ approximately), there is only one stable fixed point with zero firing rate.

- For less negative input values ($-16 < I$ approximately), there are three fixed points: two stable (low (zero) and high firing rates) and one unstable (saddle point).

The system exhibits bistability in the intermediate range of input currents.

# 3 ND network: Hopfield neural network

## 3.1 Invent a pattern

I begun by creating a specific pattern to store in our Hopfield network. For this experiment, I chose to create a simple 'X' pattern in an 8×8 grid. Each element in the pattern is either +1 or -1, represented visually as white or black pixels.

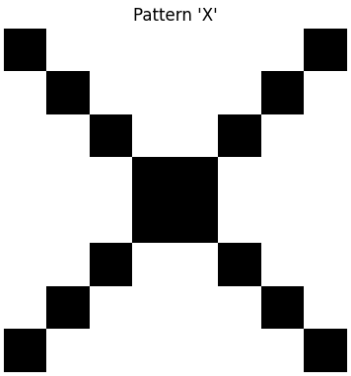


Figure 10: Visual representation of the 'X' pattern stored in the network.

The pattern is created as a 64-dimensional vector where each component takes the value +1 or -1 and is stored in the network's connectivity matrix using the outer product rule:

$$W_{ij} = \frac{1}{N} p_i p_j \tag{4}$$

## 3.2 Plot W and simulate the dynamics

After storing the pattern, we can visualize the weight matrix $W$, which encodes the synaptic connections between neurons. The weight matrix is constructed using the outer product of the pattern with itself, divided by the number of neurons (64):

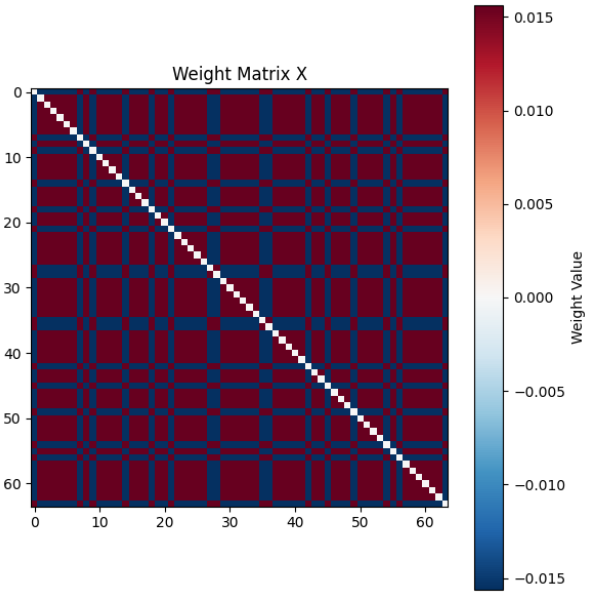


Figure 11: Visualization of the weight matrix after storing the 'X' pattern. Red indicates positive weights, blue indicates negative weights.

The weight matrix shows the correlations between neurons based on the stored pattern. Strong positive connections (red) appear between neurons that have the same value in the pattern, while strong negative connections (blue) form between neurons with opposite values

To simulate the dynamics of the Hopfield network, we implement an Euler integration method with the following update rule:

$$x(t + \Delta t) = x(t) + \Delta t \cdot [-x(t) + f(Wx(t))] + \sigma\eta(t)\sqrt{\Delta t} \tag{5}$$

where $\Delta t = 0.1$ is the time step, and $\sigma = 0.1$ is the noise amplitude.

Starting from random initial conditions, we examine how the network evolves over time:

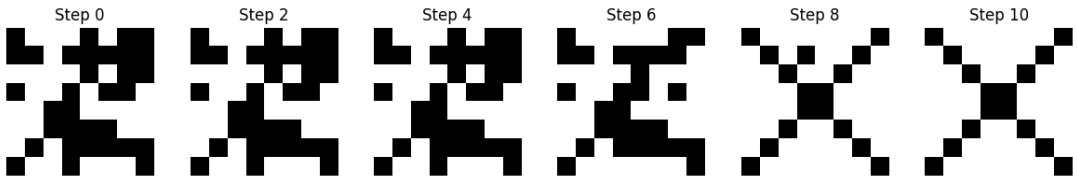


Figure 12: Evolution of network activity from random initial conditions. The network converges to the stored 'X' pattern.

The figure illustrates the temporal evolution of the network state from random initial conditions. Over time, the network activity converges toward the stored pattern, demonstrating the attractor dynamics of Hopfield networks.

## 3.3 Fixed points

Running multiple simulations with different random initial conditions reveals consistent convergence behavior:

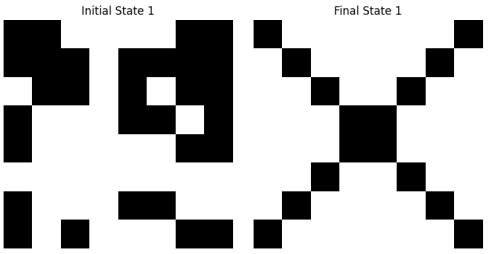


(a) Initial State 1 (b) Final State 1

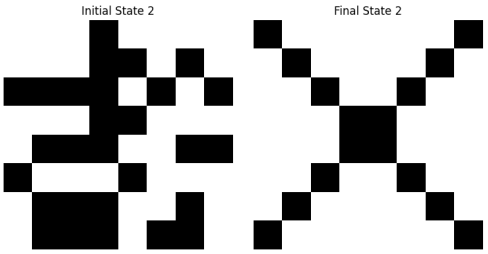


(c) Initial State 2 (d) Final State 2

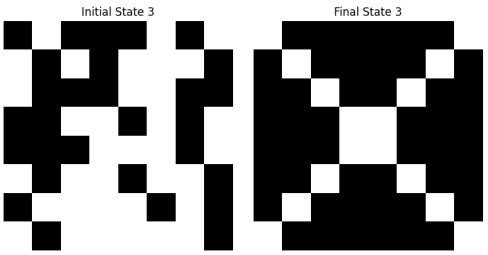


(e) Initial State 3 (f) Final State 3

Figure 13: Three simulations with different random initial states. All converge to fixed points close to the stored 'X' pattern.

Multiple simulations with different initial conditions revealed the fixed points of the system. As predicted by theory, with one stored pattern $p$, the network exhibits two fixed points: the pattern itself and its negative ($-p$).

The stability of these fixed points was evident from the convergence behavior of the network. All initial states converged to one of these fixed points, depending on which basin of attraction they started in. This behavior is characteristic of associative memory systems.

## 3.4 Introduce a new pattern

To test multiple pattern storage, I created and added a second pattern—a smiley face (☺)—to the network:

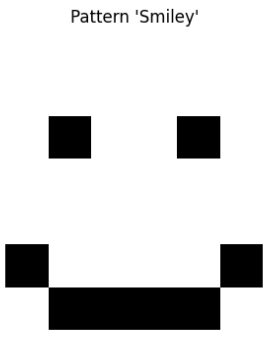


Figure 14: Visual representation of the second pattern (☺) stored in the network.

After adding the second pattern, the weight matrix was updated according to:

$$W = \frac{1}{N}(pp^T + qq^T) \tag{6}$$

where $p$ is the 'X' pattern and $q$ is the ☺ pattern.

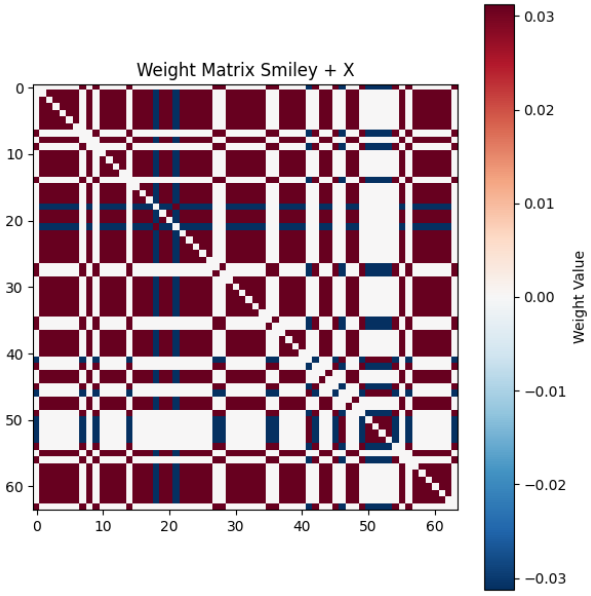


Figure 15: Updated weight matrix after storing both 'X' and ☺ patterns.

The updated weight matrix now encodes information about both patterns, with more complex connection patterns reflecting the correlations between neurons in both stored patterns.

### 3.4.1 Dynamics with Multiple Patterns

With two stored patterns, the network exhibits four potential fixed points: the two patterns and their negatives. The convergence behavior became more complex, as initial states could now be attracted to any of these fixed points based on their proximity in the state space.

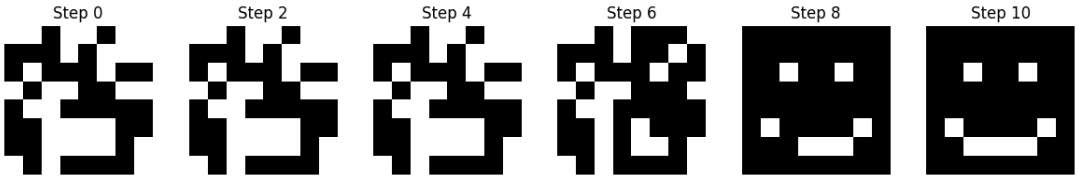


(a) Evolution of network activity from random initial conditions converging to the smiley pattern.

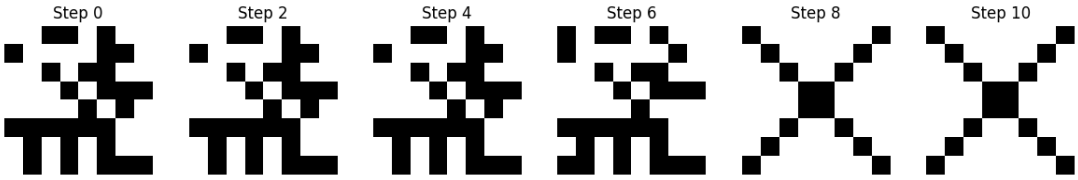


(b) Evolution of network activity from different random initial conditions converging to the X pattern.

Figure 16: Network dynamics with two stored patterns. Different initial conditions lead to convergence to different stored patterns, demonstrating multiple attractor basins in the network.

These results demonstrate that with multiple patterns stored, the network state space contains multiple attractors, and the dynamics converge to the attractor basin of the pattern most similar to the initial conditions.

## 3.5 Initial conditions

One of the key properties of Hopfield networks is their ability to recover patterns from corrupted or noisy inputs. I tested this by creating a corrupted version of the 'X' pattern with 30% of its bits flipped:

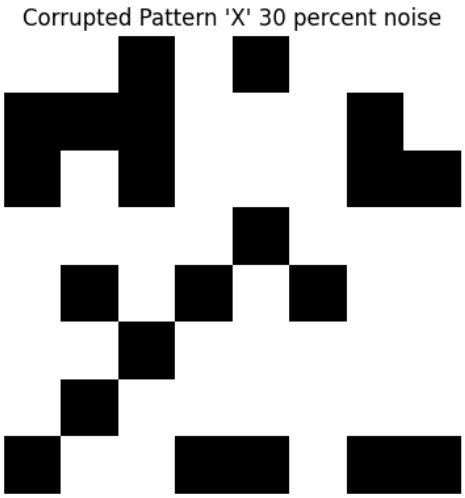


Figure 17: The 'X' pattern corrupted with 30% noise.

Using this corrupted pattern as the initial state, I simulated the network dynamics:

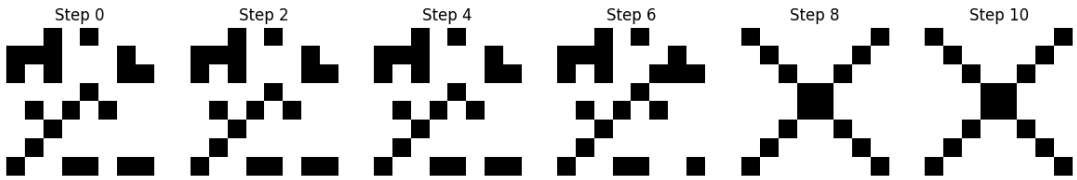


Figure 18: Network dynamics starting from the corrupted pattern. The network successfully recovers the original pattern.

The network successfully recovered the original pattern, demonstrating the error-correction capabilities of the Hopfield network.

## 3.6 Network capacity

The theoretical storage capacity of a Hopfield network is approximately $0.138N$ patterns, where $N$ is the number of neurons. For our network with $N = 64$, this gives a theoretical capacity of about 9 patterns.

To empirically test the network's capacity, I conducted multiple trials with an increasing number of random patterns stored in the network. For each pattern count, I measured the recovery success rate by corrupting each pattern and checking if the network could successfully recover it:

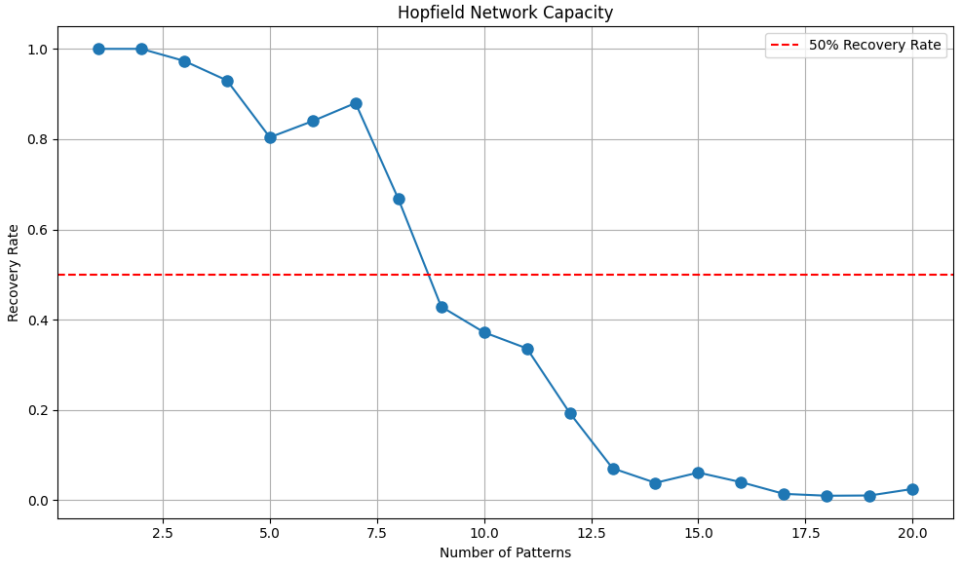


Figure 19: Network capacity curve showing recovery rate vs. number of stored patterns.

The results show that the recovery rate remains high (above 95%) when storing up to approximately 7-8 patterns. Beyond that, the recovery rate drops rapidly, crossing the 50% threshold at around 9 patterns, which aligns well with the theoretical capacity of $0.138 \times 64 \approx 9$ patterns.

This decline in performance occurs because as more patterns are stored, they begin to interfere with each other in the weight matrix, creating spurious attractors and reducing the basin of attraction for each stored pattern.

# 4 Conclusion

Summary of main findings and their significance.